In vivo and *in situ* imaging of head and neck squamous cell carcinoma using near-infrared fluorescent quantum dot probes conjugated with epidermal growth factor receptor monoclonal antibodies in mice

KAI YANG[1], CHENG ZHAO[1], YU-AN CAO[2], HONG TANG[1], YUN-LONG BAI[1], HAO HUANG[1], CHUEN-RONG ZHAO[1], RUI CHEN[1] and DAN ZHAO[1]

[1]Department of Oral and Maxillofacial Surgery, The First Affiliated Hospital, Chongqing Medical University, Chongqing 400016; [2]Department of Stomatology, Second Affiliated Hospital of Soochow University, Suzhou 215004, P.R. China

Received December 19, 2011; Accepted January 20, 2012

DOI: 10.3892/or.2012.1705

Abstract. In this study, we applied near-infrared fluorescent quantum dots (NIRF-QDs) for non-invasive *in vivo* and *in situ* imaging of head and neck squamous cell carcinoma (HNSCC). The U14 squamous cancer cell line with high expression of epidermal growth factor receptor (EGFR) was implanted subcutaneously into the head and neck regions of nude mice to establish HNSCC models. NIRF-QDs with an emission wavelength of 800 nm (NIRF-QD800) were conjugated with EGFR monoclonal antibodies to develop the QD800-EGFR Ab probe. *In vivo* and *in vitro* studies demonstrated that the QD800-EGFR Ab probe can specifically bind EGFR expressed on U14 cells. U14 squamous cell carcinoma in the head and neck can be clearly visualized by *in vivo* imaging after intravenous injection of QD800-EGFR Ab probes. The results suggested that *in situ* imaging using NIRF-QD-EGFR Ab probes has unique advantages and prospects for the investigation of tumor development, early diagnosis and personalized therapy of HNSCC.

Introduction

Non-invasive *in vivo* and *in situ* imaging of tumor cells plays an important role in studying the occurrence and development of cancers, making early diagnosis and conducting personalized therapies. This has been a difficult area due to the lack of highly sensitive imaging substances and specific marker for each particular type of tumor. Quantum dots (QDs) were developed recently and have shown great prospect in the non-invasive imaging of tumors (1,2).

QD is a type of nanocrystal composed of elements belonging to II-VI or III-V groups with a diameter of 2-10 nm. In comparison to the conventional organic fluorescent dyes and fluorescent proteins, QDs have unique optical properties, e.g., broad and continuous distribution of the excitation spectrum, narrow and symmetric emission spectrum, strong fluorescence and high photochemical stability. In addition, QDs are less prone to photobleaching and the spectrum of any points from ultraviolet to the near infrared can be obtained by changing the size and composition of QDs (3,4). These optical properties are not owned by all the current fluorescent probes. Currently, QDs have been applied in the imaging of biological macromolecules and cells both *in vitro* and *in vivo* (5-7). Non-invasive *in vivo* imaging has been used for the investigation of tumor development (8-10), early diagnosis of cancer (10), the transportation of drugs *in vivo* (11), and monitoring of therapeutic responses *in vivo* (11-13). These studies have demonstrated the unique advantages of QDs in the imaging of cells both *in vitro* and *in vivo*. Particularly, the recently developed near-infrared fluorescent quantum dot (NIRF-QD) with an emission range of 700-900 nm has the advantage of avoiding the interference of tissue auto fluorescence (400-600 nm). NIRF-QDs have strong tissue penetration, but do not have radiation and are not harmful *in vivo*. Therefore, NIRF-QDs are extremely suitable for non-invasive *in vivo* imaging (14,15).

NIRF-QDs were conjugated with prostate specific membrane antigen monoclonal antibody (PSMA), Her2 monoclonal antibody and EGF monoclonal antibody, and have been used for non-invasive *in vivo* imaging of prostate cancer, breast cancer and colon cancer, respectively, in mice (16-18). The results from these studies have shown that NIRF-QD probes conjugated with monoclonal antibodies can specifically bind the corresponding antigens expressed by the tumor cells and *in vivo* imaging can be subsequently obtained. Our previous studies (10) have also shown that *in vivo* imaging can detect a minimum of 10^4 NIRF-QDs-labeled cancer cells in the presence of skin barrier, which was 100-fold higher than

Correspondence to: Dr Kai Yang, Department of Oral and Maxillofacial Surgery, The First Affiliated Hospital, Chongqing Medical University, Chongqing 400016, P.R. China
E-mail: cqfyyk@hotmail.com

Key words: head and neck cancer, quantum dot, *in vivo* imaging

the minimal detection limit of CT and MRI. These studies demonstrate that NIRF-QDs have unique advantages for early diagnosis and personalized therapy (e.g., determination of surgical margins, evaluation of the efficacy of targeted therapy, etc.). Targeting of the nano-probes to the tumors after intravenous injection is closely related to the location of the tumors. Currently, there are no studies on non-invasive *in vivo* and *in situ* imaging of head and neck tumors by using NIRF-QD conjugated with monoclonal antibodies.

The U14 squamous cancer cells in Kunming mice highly express EGFR (19,20). In this study, we first developed head and neck squamous cell carcinoma model by implanting U14 cells subcutaneously into the chin-neck region of nude mice. We then conjugated EGFR monoclonal antibody to NIRF-QDs with a maximum emission wavelength of 800 nm to produce QD800-EGFR Ab probes. *In situ* and *in vivo* imaging of U14 squamous cell carcinoma can be obtained by intravenous injection of QD800-EGFR Ab probes. To our knowledge, this is the first study that EGFR antibody-conjugated NIRF-QDs were utilized for non-invasive *in vivo* and *in situ* imaging of head and neck squamous cell carcinoma (HNSCC). The results obtained from these studies provide foundations for the application of NIRF-QDs *in vivo* imaging, personalized diagnosis and treatment of HNSCC.

Materials and methods

Cell line and animals. The U14 cell line was purchased from the Chinese Academy of Medical Sciences Cancer Institute. The cells were maintained at 37˚C in a humidified atmosphere containing 5% CO_2 in DMEM supplemented with 10% fetal bovine serum, 2 mM L-glutamine, 100 U/ml penicillin, and 100 mg/ml of streptomycin. SPF level BALB/c nu/nu nude mice (n=15, age, 6-8 weeks; weigh, 20-25 g) were purchased from the Experimental Animal Center of Chongqing Medical University and were maintained in constant temperature and humidity. Feeds, bedding and water were sterilized. All experimental procedures were approved by the Animal Administration Committee of Chongqing Medical University.

Preparation and purification of QD800-EGFR Ab probes. QD800-EGFR Ab probes were prepared using Qdot® Antibody Conjugation Kits (Invitrogen, Carlsbad, CA, USA) according to the manufacturer's instruction. The first step was the activation and elution of QDs. In this step, 14 μl SMCC at the concentration of 10 mM was mixed with 125 μl QD800 (amine-functionalized CdSeTe/ZnS) at the concentration of 4 μM. After activation at room temperature for 1 h, the mixture was loaded onto NAP-5 column and the colored elution (500 μl) was collected. The second step was antibody reduction and separation. In this step, 6.1 μl DTT (1 M) was added into 300 μl EGFR monoclonal antibody (Abcam, UK) (1 mg/ml in PBS). After 30-min reduction reaction, dye indicator was added and colored solution (500 μl) was obtained by eluting from NAP-5 column. The third step was conjugation and inactivation. In this step, elutions collected in step 1 and 2 were mixed, and after 1-h conjugation, 3 μl 2-mercaptoethanol (10 mM) was added for 30-min inactivation. The final step was concentration and purification. In this step, the inactivated solutions were added into ultrafiltration tube. After 15 min of ultracentrifugation at 7,000 rpm, the conjugated solution was collected from the inner side of the ultrafiltration membrane. The conjugated solution was separated by chromatography and the purified QD800-EGFR Ab probes were obtained. The concentration of QD800-EGFR Ab probes was calculated by the equation: $A = \varepsilon cl$, where A represent absorbance, ε represent the extinction coefficient, c represent the molar concentration and l represent the optical path.

The extinction coefficient at 550 nm (ε_{550}) of the purified QD800-EGFR Ab probes was 1.7×10^6 $(mol/l)^{-1}cm^{-1}$. Absorbance was measured by UV spectrophotometer (Beckman, DU-600) at 550 nm and the value was 3.442 and the optical path (l) was 1 cm. According to the equation described in Materials and methods, the concentration of the purified QD800-EGFR Ab probes was 2.025 μM.

In vitro labeling of U14 cells by QD800-EGFR Ab probes. Well-grown U14 cells were inoculated into 9 35-mm glass bottom culture dishes (ø 15 mm) at a concentration of 5×10^4/dish. After 24 h of culture, the medium was discarded, and the cells were washed with PBS 3 times. The cells were divided into 3 groups. In the experimental group, the cells were added with 100 μl QD800-EGFR Ab probes (100 nM). The cells in the control group I were added with 100 μl QD800 (100 nM). The cells in the control group II were added with 200 μl EGFR monoclonal antibody (1 μg/ml) to block EGFR. After 2 h of incubation, the cells were washed with PBS 3 times and then added with 100 μl QD800-EGFR Ab probes (100 nM). The cells in each group after addition of QD800-EGFR Ab probes or QD800 were incubated at 37˚C for 30 min followed by 3 washes with PBS. The QD800-EGFR Ab probe-labeled U14 cells were observed under a confocal laser scanning microscope (Leica, TCS-SP5). The following scanning parameters were used: excitation, 405 nm; emission, 750-800 nm; image acquisition size, 1024x1024 pixels; speed, 400 HZ; pinhole size, 135.9 μM; line average, 4; frame average, 1; zoom, 2.0; Scan-Direction, 2; resolution, 8 bits.

Development of HNSCC model in nude mice. Logarithmic growth phase U14 cells were trypsinized by 0.5% trypsin. After centrifugation at 4˚C (800 rpm) for 4 min, the cells were resuspended in PBS. The suspension containing 2×10^6 U14 cells were injected subcutaneously into the chin-neck junction area of 15 nude mice to establish the HNSCC model. Tumor growth was observed daily and the experiment started when the maximum diameter of the tumor reached 0.8-1.2 cm.

In vivo imaging of the tumors. The mice with tumors were divided into experimental group, control group I and control group II with 5 mice in each group. After anesthesia by intraperitoneal injection of 2% sodium pentobarbital (40 mg/kg), each mouse in the experimental group was injected with 100 μl QD800-EGFR Ab probes containing 100 pmol equivalent of QD800 via the tail vein. For the control group I, each mouse was injected with 100 μl of QD800 containing 100 pmol equivalent of QD800 via the tail vein. Each mouse in the control group II was injected with 250 μl EGFR monoclonal antibody (1 mg/ml) to block EGFR. After 24 h, the mice were injected with 100 μl QD800-EGFR Ab probe containing 100 pmol equivalent of QD800 via the tail vein. *In vivo* imaging was

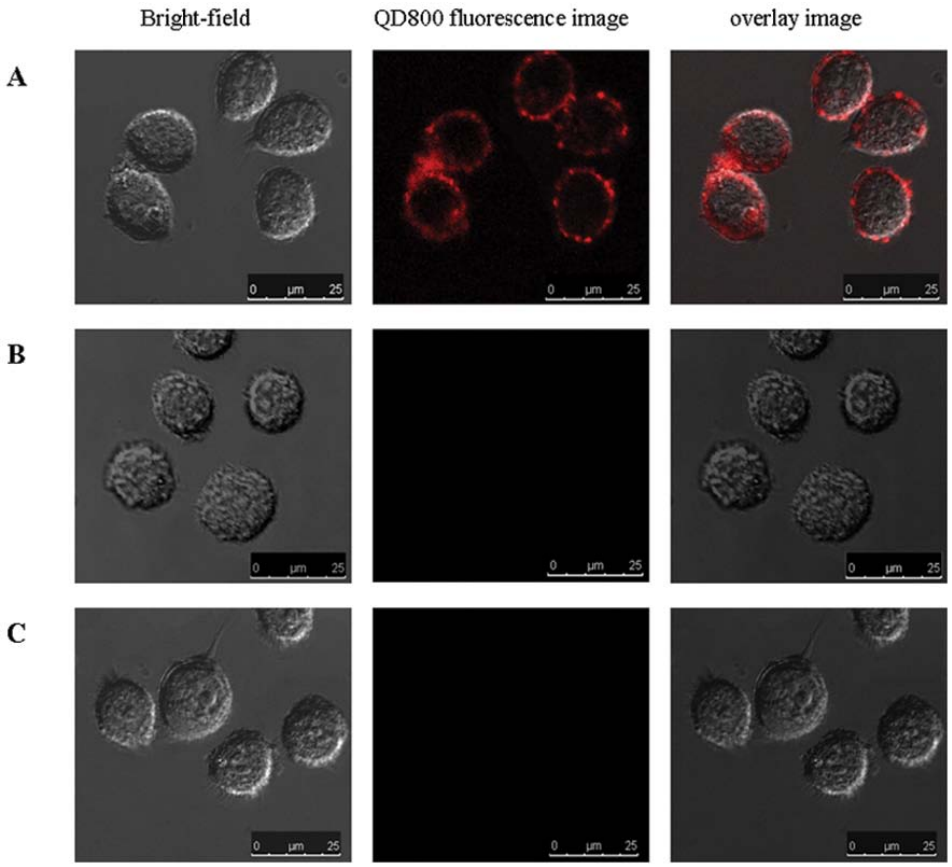

Figure 1. Fluorescent images of U14 cells after 30 min of labeling with QD800-EGFR Ab probes. (A) Experimental group in which the cells were added with QD800-EGFR Ab probes; (B) control group I in which the cells were added with QD800; (C) control group II in which the cells were added with 200 μl EGFR monoclonal antibody (1 μg/ml) to block EGFR. After 2 h of incubation, the cells were washed with PBS 3 times and then added with 100 μl QD800-EGFR Ab probes (100 nM). All images were acquired under the same conditions (excitation/emission, 405/750-800 nm) and displayed on the same scale (scale bar, 25 μm).

conducted for all the animals after 30 min, 1, 3, 6, 9 and 24 h of injection of the QD800-EGFR Ab probes or QD800 using Maestro In Vivo imaging system (CRI). Excitation/emission wavelength was 630/800 nm, the exposure time was 50 ms and the acquisition time was 10 sec with a binning of 2x2 and pixels of 1024x1024. All the images were processed and the data were analyzed by Maestro2.10.0 software. Auto- and the target-fluorescence were detected and each signal was assigned with a pseudo-color. Auto-fluorescence in this study was set to green color and the target signal was set to red color. Finally, overlay of the two color images were used for analysis.

Cellular and histological examination of the U14 tumors. Two mice from the experimental group, control group I and control groups II, respectively, were euthanized 6 h after injection of QD800-EGFR Ab probe and QD800. The remaining 3 mice from the experimental and control groups were euthanized 24 h after of QD800-EGFR Ab probe injection. The subcutaneous neck tumors were excised and embedded in Optimal Cutting Temperature compound. The embedded samples were frozen and cryo-sections with a thickness of 7 μm were continuously cut at -20˚C. One of every two continuous sections was stained with hematoxylin and eosin (H&E) for observation of the tumor growth. The other section was used for confocal microscopy analysis to observe the distribution of QD800 in the tissues. Confocal parameter settings were the same as described above.

Statistical analysis. Statistical analysis was performed using paired and unpaired Student's t-tests for comparisons between and within groups, respectively. Statistical significance was established at the level of $P<0.05$. Data are presented as the means ± SE.

Results

In vitro labeling of U14 cells by QD800-EGFR Ab probes. Red fluorescence of QD800 was observed on the membrane of U14 cells in the experimental group (Fig. 1A). In contrast, fluorescence was not observed in the cells of control group I or control group II (Fig. 1B and C), suggesting that QD800 does not bind U14 cells, while QD800-EGFR Ab probes can bind U14 cells. In addition, QD800-EGFR Ab probes did not bind U14 cells that had been blocked by EGFR monoclonal antibody. These results demonstrated that the immunological activity of EGFR Ab was maintained after conjugation with QD800 and could specifically recognize EGFR expressed on the surface of U14 cells, leading to the attachment of QD800 to the cell surface.

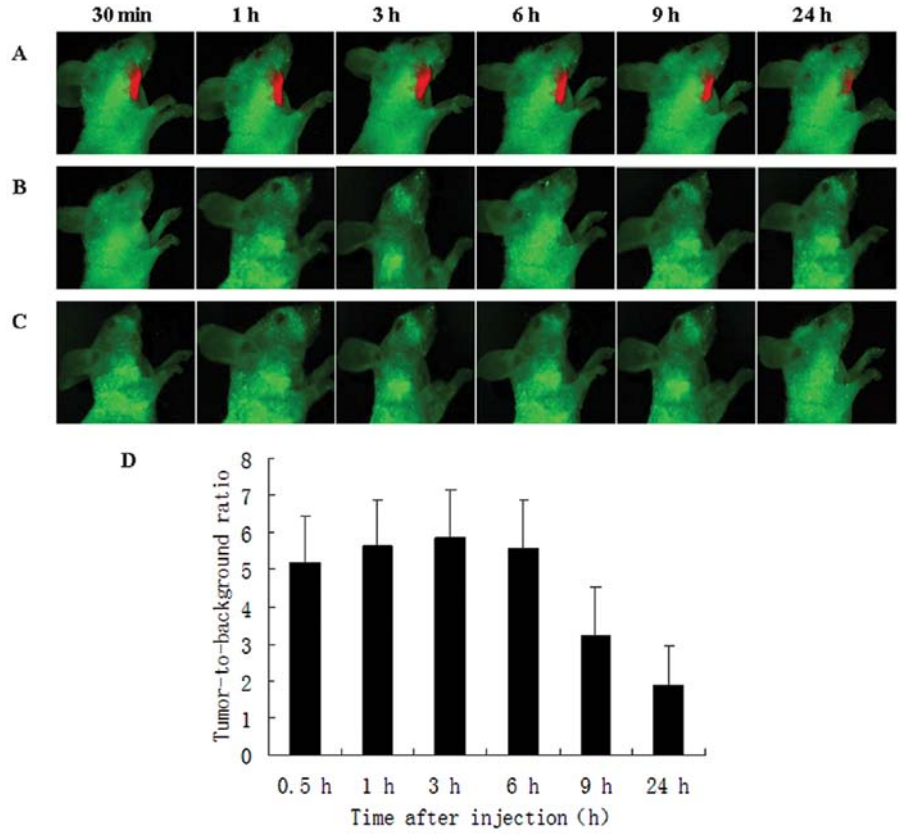

Figure 2. *In vivo* imaging of tumors by QD800-EGFR Ab probes at different times points. (A) *In vivo* images of U14 squamous cell carcinoma mice after intravenous injection with QD800-EGFR Ab probe in the experimental group; (B) *in vivo* images of U14 squamous cell carcinoma mice after intravenous injection with 100 pmol QD800 in the control groupI; (C) *in vivo* images of U14 squamous cell carcinoma mice in the control group II, the mice were injected with 250 μl EGFR monoclonal antibody (1 mg/ml) and 24 h later the mice were injected with 100 l QD800-EGFR Ab probes containing 100 pmol equivalent of QD800; (D) the changes of the signal-to-noise ratio at different time points after injection of the probe for *in vivo* imaging of U14 squamous cell carcinoma in the experimental group.

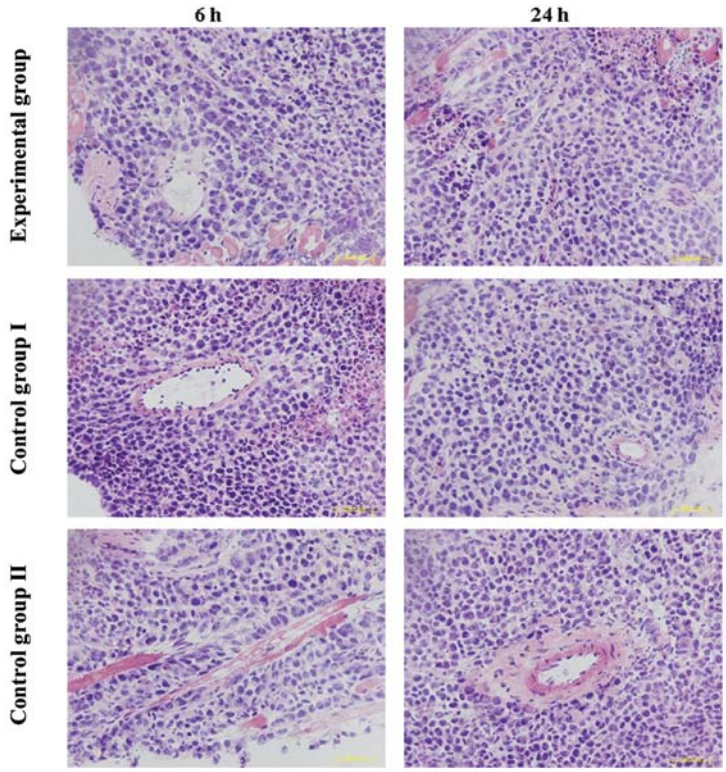

Figure 3. Hematoxylin and eosin staining of tumor sections. H&E staining of tumor section from the experimental group, control group I and control group II of U14 squamous cell carcinoma after 6 and 24 h of probe injection.

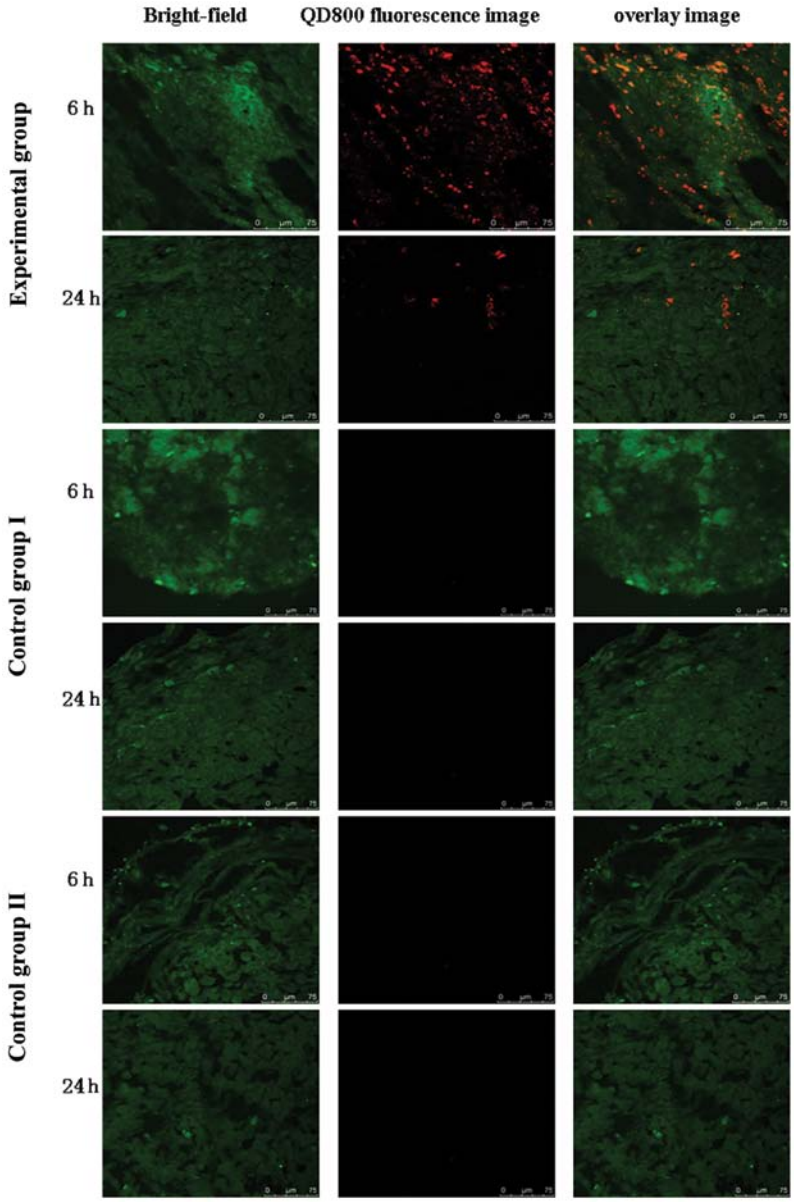

Figure 4. Distribution of fluorescence signals in tumors. Laser Scanning Confocal Microscope analysis of tumor frozen tissue sections from the experimental group, control group I and control group II of U14 squamous cell carcinoma after 6 and 24 h of probe injection (scale bar, 75 μM).

In vivo imaging of tumors. Significant tumor growth was observed 1 week after inoculation with U14 cells in the chin-neck junction area of nude mice. Tumors developed in all the 15 nude mice. Two weeks after inoculation, the maximum diameter of the tumors reached 0.8-1.2 cm and at this time point we started the imaging experiment. The tumor sites of mice in the experimental group showed significant fluorescent signals 30 min after injection of QD800-EGFR Ab probes via the tail vein. The most complete fluorescent signals were observed after 30 min to 6 h of probe injection and the size of the fluorescent images corresponded to that of the tumors. The size of the fluorescent images was significantly reduced after 9 h of probe injection and the fluorescent images were minimal after 24 h of probe injection (Fig. 2A). The signal-to-noise ratio (the fluorescence intensity ratio between tumor and background) was relatively high from 30 min to 6 h after probe injection. The signal-to-noise ratio was significantly decreased at 9 h and was close to the baseline level at 24 h after probe injection (Fig. 2D). In the control group I and control group II, fluorescent signals were not detected at the tumor sites after 30 min to 24 h of probe injection (Fig. 2B and C).

Cellular and histological examination of the U14 tumors. H&E staining of the tumor sections from the mice after 6 h and 24 h of probe injection showed that there were large amount of cancer cells in the tumors of both experimental and control groups, suggesting that tumors were well developed (Fig. 3). Confocal microscopy analysis of the cryo-sections confirmed that QD800 fluorescence signal was not detected in the tumor section of mice in the control group I and control group II after 6 h and 24 h of injection. In contrast, in the experimental group, large amount of QD800 was accumulated in the tumor section of mice after 6 h of injection. QD800 was scattered in the tumor section of mice after 24 h of injection (Fig. 4).

Discussion

Direct *in vivo* and *in situ* imaging of cancer cells is one of the key technologies for investigation of tumor development, early diagnosis, drug screening and personalized treatment (9,10,21,22). In comparison to the existing organic fluorescent dyes and fluorescent proteins, QDs have excellent optical properties, e.g., high light stability and high fluorescence quantum yields. Particularly, NIRF-QDs have excellent tissue penetration and great prospects for non-invasive *in vivo* imaging of the cancer cells (1-4). Previous studies have demonstrated that QDs at the experimental concentration are not cytotoxic and do not affect the growth and differentiation of the live cells (3,4,23). Our previous studies have also shown that labeling of cancer cells with NIRF-QDs do not affect their growth, proliferation, apoptosis, invasion, metastasis or the ability to form tumors (10,24-26). Clinically, optical examination is a safe, simple and economical approach (18,27). In addition to the unique optical properties as described earlier. QDs, as nanoparticles, have an easily modified surface, can be connected to variety of biological molecules and can easily penetrate tumor angiogenesis and reach the cancer cells (10,16-18). Therefore, QDs have shown unique advantages for non-invasive *in vivo* imaging of cancers.

One of the difficult problems in surgical treatment is how to correctly identify the tumor boundary and determine the scope of tailored surgical resection for different patients to improve their survival rate and quality of life. Since there is no method for direct visualization of cancer cells during surgery, clinicians determine the surgery boundary by experience and the alteration of the cancer tissue texture, which leads to a failure rate of as high as 40% in patients with complete removal of head and neck cancer surgery (28,29) and greatly affects the patients' survival rate. Therefore developing methods by which clinicians could monitor cancer cells in real time during surgery and perform individual tailored surgical resection is one of the key technologies to improve survival. In this study, we implanted U14 squamous cancer cells with high expression of EGFR into the head and neck sites of nude mice for *in vivo* imaging studies. This was due: 1), most of the malignant tumors in the head and neck regions are squamous cell carcinoma and 90% of the squamous cancer cells highly express EGFR (30,31). Therefore, QD *in vivo* imaging by targeting EGFR has broad applicability for HNSCC; 2), targeting of EGFR antibody-conjugated QDs (a kind of nano-probe) to the tumors after intravenous injection is closely related to the location of the tumors and currently there are no reports with regard to the QDs *in vivo* imaging of head and neck tumors.

In this study, we conjugated NIRF-QDs with EGFR monoclonal antibody to produce QD800-EGFR Ab probes. Our results demonstrated that QD800-EGFR Ab probes can specifically bind U14 squamous cancer cells both *in vivo* and *in vitro* and produce clear images of head-neck tumors. Imaging of U14 squamous cell carcinoma by QD800-EGFR Ab probes is achieved by both active and passive targeting (18,32). The tumor is rich in angiogenesis. The basal membrane of tumor angiogenesis is incomplete or lacking and there are wide gaps between the endothelial cells. The presence of these gaps results in the passive targeting of the QD800-EGFR Ab probes into the tumor tissues through the highly permeable tumor angiogenesis. Specific antigen-antibody binding leads to the active targeting of QD800-EGFR Ab probes to the EGFR on cell surface. Thus, EGFR Ab acts as a bridge to connect QD800 to the cells. Our studies showed that the bright and complete fluorescence images are not significantly changed from 30 min to 6 h in the experimental group after intravenous injection of QD800-EGFR Ab probes. However, the size and intensity of the fluorescence images are significantly decreased after 9 h of probe injection, indicating that the best time for imaging of HNSCC by QD800-EGFR Ab probes is from 30 min to 6 h after intravenous injection of the probes. After 24 h of probe injection, the images of the tumors are further reduced and the intensity of fluorescence is decreased. This might be due to the gradual degradation of ligands and coating layer on the surface of probe by lysosomal enzymes (18,32,33), leading to gradual decreases of the probe binding ability and gradual quenching of the fluorescent quantum dots. Our previous studies (10) have also shown that *in vivo* imaging can detect a minimum of 10^4 cancer cells labeled with NIRF-QDs in the presence of skin barrier, which was 100-fold higher than the minimal detection limit of CT and MRI. In addition, the sensitivity can be further enhanced when the tumor is exposed during surgery. Gao *et al* predicted (32) that *in vivo* imaging can detect as low as 10-100 QDs-labeled cancer cells. In this study, toxicity of the ODs in the mice was not observed.

This study demonstrates that intravenous injection of QD800-EGFR Ab probes can produce clear *in vivo* and *in situ* images of HNSCC with high expression of EGFR. QD800-EGFR Ab probes have shown great potential in the investigation of tumor development, early diagnosis and its individual tailored surgical resection. Previous studies have suggested that biologically functionalized QDs have excellent biological compatible and are water soluble (3,4,23). In addition, they do not cause side effects on live subjects and do not affect cellular growth, differentiation and function within the range of experimental doses (3,4,10,23-26). However, the core of QDs is typically made up of heavy metal elements, e.g., plutonium, cadmium and mercury. These metal elements are toxic when they are released. Though the toxicity of these QDs can be reduced by using core-shell structure, long-term *in vivo* biological oxidation and degradation may cause QD shell shedding, which can lead to the release of heavy metal ion and subsequent toxic action (34). Therefore, the studies of replacing plutonium, cadmium or mercury with other elements to produce non-toxic QDs or speeding up excretion of QDs from body are important directions for future investigations.

Acknowledgements

The study was supported by the National Natural Science Foundation of China (No. 81172205; 30872925).

References

1. Bentolila LA, Ebenstein Y and Weiss S: Quantum dots for in vivo small-animal imaging. J Nucl Med 50: 493-496, 2009.
2. Ciarlo M, Russo P, Cesario A, Ramella S, Baio G, Neumaier CE and Paleari L: Use of the semiconductor nanotechnologies 'quantum dots' for in vivo cancer imaging. Recent Pat Anticancer Drug Discov 4: 207-215, 2009.

3. Michalet X, Pinaud FF, Bentolila LA, Tsay JM, Doose S and Li JJ: Quantum dots for live cells, in vivo imaging, and diagnostics. Science 307: 538-544, 2005.
4. Medintz IL, Uyeda HT, Goldman ER and Mattoussi H: Quantum dot bioconjugates for imaging, labelling and sensing. Nat Mater 4: 435-446, 2005.
5. Smith AM, Gao X and Nie S: Quantum dot nanocrystals for in vivo molecular and cellular imaging. Photochem Photobiol 80: 377-385, 2004.
6. Gao X, Yang L, Petro JA, Marshall FF, Simons JW and Nie S: In vivo molecular and cellular imaging with quantum dots. Curr Opin Biotechnol 16: 63-72, 2005.
7. Smith AM, Duan H, Mohs AM and Nie S: Bioconjugated quantum dots for in vivo molecular and cellular imaging. Adv Drug Deliv Rev 60: 1226-1240, 2008.
8. Wang C, Gao X and Su X: In vitro and in vivo imaging with quantum dots. Anal Bioanal Chem 4: 1397-1415, 2010.
9. Byers RJ and Hitchman ER: Quantum dots brighten biological imaging. Prog Histochem Cytochem 45: 201-237, 2011.
10. Cao Y, Yang K, Li Z, Zhao C, Shi C and Yang J: Near-infrared quantum-dot-based non-invasive in vivo imaging of squamous cell carcinoma U14. Nanotechnology 2: 475104, 2010.
11. Mamot C, Drummond DC, Noble CO, Kallab V, Guo Z, Hong K, Kirpotin DB and Park JW: Epidermal growth factor receptor-targeted immunoliposomes significantly enhance the efficacy of multiple anticancer drugs in vivo. Cancer Res 65: 11631-11638, 2005.
12. Koo H, Huh MS, Ryu JH, Lee DE, Sun IC and Choi K, Kim K and Kwon IC: Nanoprobes for biomedical imaging in living systems. Nano Today 6: 204-220, 2011.
13. Kobayashi H and Choyke PL: Target-cancer-cell-specific activatable fluorescence imaging probes: rational design and in vivo applications. Acc Chem Res 44: 83-90, 2010.
14. Aswathy RG, Yoshida Y, Maekawa T and Kumar DS: Near-infrared quantum dots for deep tissue imaging. Anal Bioanal Chem 397: 1417-1435, 2010.
15. Jiang W, Singhal A, Kim BYS, Zheng J, Rutka JT and Wang C: Assessing near-infrared quantum dots for deep tissue, organ, and animal imaging applications. J Assoc Lab Autom 13: 6-12, 2008.
16. Shi C, Zhu Y, Xie Z, Qian W, Hsieh CL and Nie S: Visualizing human prostate cancer cells in mouse skeleton using bioconjugated near-infrared fluorescent quantum dots. Urology 74: 446-451, 2009.
17. Tada H, Higuchi H, Wanatabe TM and Ohuchi N: In vivo real-time tracking of single quantum dots conjugated with monoclonal anti-HER2 antibody in tumors of mice. Cancer Res 67: 1138-1144, 2007.
18. Diagaradjane P, Orenstein-Cardona JM, Colón-Casasnovas NE, *et al*: Imaging epidermal growth factor receptor expression in vivo: Pharmacokinetic and biodistribution characterization of a bioconjugated quantum dot nanoprobe. Clin Cancer Res 14: 731-741, 2008.
19. DiSilvestro PA, Walker JL, Morrison A, Rose PG, Homesley H and Warshal D: Radiation therapy with concomitant paclitaxel and cisplatin chemotherapy in cervical carcinoma limited to the pelvis: a phase I/II study of the Gynecologic Oncology Group. Gynecol Oncol 103: 1038-1042, 2006.
20. Slichenmyer WJ and Fry DW: Anticancer therapy targeting the erbB family of receptor tyrosine kinases. Semin Oncol 28: 67-79, 2001.
21. Lee S, Park K, Kim K, Choi K and Kwon IC: Activatable imaging probes with amplified fluorescent signals. Chem Commun 36: 4250-4260, 2008.
22. Koo H, Lee H, Lee S, Min KH, Kim MS and Lee DS: In vivo tumor diagnosis and photodynamic therapy via tumoral pH-responsive polymeric micelles. Chem Commun 46: 5668-5670, 2010.
23. Jaiswal JK, Mattoussi H, Mauro JM and Simon SM: Long-term multiple color imaging of live cells using quantum dot bioconjugates. Nat Biotechnol 21: 47-51, 2003.
24. Yang K, Li Z, Cao Y, Yu X and Mei J: Effect of peptide-conjugated near-infrared fluorescent quantum dots (NIRF-QDs) on the invasion and metastasis of human tongue squamous cell carcinoma cell line Tca8113 in vitro. Int J Mol Sci 10: 4418-4427, 2009.
25. Li ZG, Yang K, Cao YA, Zheng G, Sun DP and Zhao C: In vivo study of the effects of peptide-conjugated near-infrared fluorescent quantum dots on the tumorigenic and lymphatic metastatic capacities of squamous cell carcinoma cell line Tca8113 and U14. Int J Mol Sci 11: 1413-1422, 2010.
26. Sun D, Yang K, Zheng G, Li Z and Cao Y: Study on effect of peptide-conjugated near-infrared fuorescent quantum dots on the clone formation, proliferation, apoptosis, and tumorigenicity ability of human buccal squamous cell carcinoma cell line BcaCD885. Int J Nanomed 5: 401-405, 2010.
27. Chen Y, Intes X and Chance B: Development of high-sensitivity near-infrared fluorescence imaging device for early cancer detection. Biomed Instrum Technol 39: 75-85, 2005.
28. Woolgar JA and Triantafyllou A: A histopathological appraisal of surgical margins in oral and oropharyngeal cancer resection specimens. Oral Oncol 41: 1034-1043, 2005.
29. Rosenthal EL, Kulbersh BD, Duncan RD, Zhang W, Magnuson JS, Carroll WR and Zinn K: In vivo detection of head and neck cancer orthotopic xenografts by immunofluorescence. Laryngoscope 116: 1636-1641, 2006.
30. Rogers SJ, Harrington KJ, Rhys-Evans P, O-Charoenrat P and Eccles SA: Biological significance of c-erbB family oncogenes in head and neck cancer. Cancer Metastasis Rev 24: 47-69, 2005.
31. Kalyankrishna S and Grandis JR: Epidermal growth factor receptor biology in head and neck cance. J Clin Oncol 24: 2666-2672, 2006.
32. Gao X, Cui Y, Levenson RM, Chung LW and Nie S: In vivo cancer targeting and imaging with semiconductor quantum dots. Nat Biotechnol 22: 969-976, 2004.
33. Cai W, Shin DW, Chen K, Gheysens O, Cao Q and Wang SX: Peptide-labeled near-infrared quantum dots for imaging tumor vasculature in living subjects. Nano Lett 6: 6669-6676, 2006.
34. Yong KT: Mn-doped near-infrared quantum dots as multimodal targted probes for pancreatic cancer imaging. Nanotechnology 20: 015102, 2009.